Rare Met. (2018) 37(4):282–289
https://doi.org/10.1007/s12598-018-1007-0

RARE METALS
www.editorialmanager.com/rmet

Improved electrical transport properties and optimized thermoelectric figure of merit in lithium-doped copper sulfides

Meng-Jia Guan, Peng-Fei Qiu*, Qing-Feng Song, Jiong Yang,
Du-Di Ren, Xun Shi, Li-Dong Chen

Received: 8 December 2017 / Revised: 4 January 2018 / Accepted: 9 February 2018 / Published online: 2 March 2018

Abstract Copper sulfide Cu_2S is a p-type semiconducting compound that has attracted great attentions in the thermoelectric (TE) community most recently. Considering the intrinsic ultralow lattice thermal conductivity, the enhancement of TE performance in Cu_2S should be achieved through improving its electrical transport properties. To achieve this goal, lithium element was doped into Cu_2S in this study. A series of $Cu_{2-x}Li_xS$ samples with different Li contents ($x = 0$, 0.005, 0.010, 0.050, and 0.100) was synthesized by the melting–annealing method. When $x \leq 0.05$, the $Cu_{2-x}Li_xS$ samples are stable and pure phases, having the same monoclinic structure with the pristine Cu_2S at room temperature. The electrical conductivities in the $Cu_{2-x}Li_xS$ samples are greatly improved with the Li-doping content increasing due to the enhanced carrier concentrations. Meanwhile, doping Li into Cu_2S increases the ionic activation energy and lessens the influence of mobile Cu ions on the heat-carrying phonons. Thus, the thermal conductivities of the Li-doped Cu_2S samples increase. A maximal figure of merit (zT) of 0.84 at 900 K is obtained in $Cu_{1.99}Li_{0.01}S$, about 133% improvement as compared with that in Cu_2S matrix.

Keywords Thermoelectric; Copper sulfide; Doping; Superionic conductor

1 Introduction

Utilizing waste heat is critical for reducing fossil fuel consumption and decreasing CO_2 concentrations in the atmosphere. Thermoelectric (TE) technology can directly convert heat into useful electricity, showing a great potential in the applications of harvesting waste heat from industrial processes or automobiles [1–4]. The energy conversion efficiency of a TE material is evaluated by the dimensionless TE figure of merit, $zT = S^2\sigma T/\kappa$, where S is the Seebeck coefficient, σ is the electrical conductivity, T is the absolute temperature, and κ is the thermal conductivity. The quantity $S^2\sigma$ is called power factor (PF), which is associated with the electrical transport properties. To make the TE technology practically in large-scale use, the materials with high zT are required to enable high energy conversion efficiency.

Cu_2S is a p-type semiconducting compound that has attracted great attention in TE community in the past several years [5, 6]. The stoichiometric Cu_2S compound possesses two phase transitions. One is at about 370 K, and the other is at about 700 K. Below 370 K, Cu_2S is called as low-chalcocite γ phase (L-chalcocite), which is a normal solid. Between 370 and 700 K, Cu_2S crystalizes in the hexagonal β phase (H-chalcocite) [7]. Above 700 K, it further transforms to the α phase with a fcc cubic structure. The details of phase structures including lattice parameters are shown in Table 1 [8].

Both β-Cu_2S and α-Cu_2S belong to the superionic conductors, in which the sulfur atoms maintain a rigid

M.-J. Guan, P.-F. Qiu*, Q.-F. Song, D.-D. Ren, X. Shi,
L.-D. Chen
State Key Laboratory of High Performance Ceramics and
Superfine Microstructure, Shanghai Institute of Ceramics,
Chinese Academy of Science, Shanghai 200050, China
e-mail: qiupf@mail.sic.ac.cn

M.-J. Guan, Q.-F. Song
University of Chinese Academy Science, Beijing 100049, China

J. Yang
Materials Genome Institute, Shanghai University,
Shanghai 200444, China

Table 1 Crystal structures and lattice parameters of different phase structures in Cu_2S [8]

Phase	Crystal system	*a*/nm	*b*/nm	*c*/nm
γ	Monoclinic	1.529	1.193	1.358
β	Hexagonal	0.4033	/	0.6739
α	Cubic	0.5762	/	/

sublattice, while the "liquid-like" Cu ions are distributed throughout many possible positions inside the rigid sublattice with high diffusivities. On the one hand, the highly disordered diffusing copper ions strongly scatter the heat-carrying phonons, resulting in very short phonon mean free path. On the other hand, the liquid-like nature of Cu ions also effectively eliminates part transverse phonons, leading to much reduced heat capacities (C_p) which are below the limit value of 3 Nk_B (where N is the number of atoms composed of lattice and k_B is Boltzmann constant) in a normal solid. Hence, very low lattice thermal conductivity (κ_L), about 0.3 $W{\cdot}m^{-1}{\cdot}K^{-1}$, was obtained in Cu_2S [9]. As a result of such low κ_L, a maximum zT of 0.6 was achieved in Cu_2S at 1000 K in spite of the relatively low carrier concentration (p) ($\sim 1\times10^{18}$ cm^{-3}) and small σ ($\sim 1\times10^3$ $S{\cdot}m^{-1}$) [9]. Considering that the elements are low cost, nontoxic, and earth-abundant, Cu_2S becomes a potential candidate which can be used in the waste heat recovery industry.

Optimizing the electrical transport properties and reducing the κ are two common strategies to improve the zT of established TE materials [10–12]. Considering the intrinsic ultralow κ_L, improving the zT of Cu_2S should focus on the optimization of electrical transport properties, especially enhancing its p. The binary phase diagram of Cu–S shows that the Cu composition in cubic $Cu_{2-\delta}S$ phase can be down to $\delta = 0.27$ at 780 K [7]. Thus, introducing Cu-deficiency is an effective way to generate additional holes to enhance the p. When the Cu-deficiency content $\delta = 0.03$, the p at 300 K is increased to 7.3×10^{20} cm^{-3}, about two orders of magnitude higher than the that of stoichiometric Cu_2S. Meanwhile, the intrinsic ultralow κ_L can be well maintained in the Cu-deficient $Cu_{2-\delta}S$ compounds. Consequently, a record-high zT of 1.7 at 1000 K has been achieved in $Cu_{1.97}S$ [9]. Further increasing Cu-deficiency can continuously enhance the p. When the Cu-deficiency content $\delta = 0.2$, the p is as high as 5.4×10^{21} cm^{-3} at 300 K [13]. However, such high p significantly deviates the optimal p range, thus the zTs are poor for these $Cu_{2-\delta}S$ samples with large content of Cu-deficiency [13]. Beyond introducing Cu-deficiency, doping the foreigner elements is also a very familiar way to tune the electrical transport properties of established TE materials [14–16]. However, very little work has been performed on doping the foreigner elements in Cu_2S to optimize the electrical transport properties. Actually, so far, Li is the only electropositive element which was reported to be doped into Cu_2S successfully. In 2004, Balapanov et al. [17] fabricated several $Cu_{2-x}Li_xS$ ($0 < x < 0.25$) compounds and measured their ionic conductivities. It is found that Li dopants can decrease the ionic conductivity by increasing the ionic activation energy. Nevertheless, the TE properties of these Li-doped Cu_2S compounds have not been characterized. Most recently, Kang et al. [18] investigated the TE properties of Li-doped Cu_2Se compounds. They found that doping Li at Cu-sites can increase the σ and then improve the zT. Similar phenomenon might also happen in Cu_2S system.

In this study, a series of $Cu_{2-x}Li_xS$ samples with different Li-doping contents ($x = 0$, 0.005, 0.010, 0.050, and 0.100) were synthesized. Their electrical and thermal transport properties were measured in the temperature range from 300 to 900 K. A systematic evaluation about the effect of Li doping at Cu-sites on crystal structure and TE properties was performed. As a result of the optimized electrical transport properties, a maximal zT of 0.84 at 900 K was obtained in $Cu_{1.99}Li_{0.01}S$, about 133% improvement as compared with that in Cu_2S matrix.

2 Experimental

Polycrystalline $Cu_{2-x}Li_xS$ ($x = 0$, 0.005, 0.010, 0.050, and 0.100) samples were prepared by melting-quenching-annealing method. High-purity raw elements Cu (shots, 99.999%, Alfa Aesar), S (pieces, 99.999%, Alfa Aesar), and Li (ingot, 99.999%, Sigma-Aldrich) were weighted out in stoichiometric proportions and then sealed in carbon-coated silica tubes under a vacuum level of − 100 kPa. The sealed tubes were slowly raised to 923 K and dwelled for 4 h, and then continually raised to 1383 K and dwelled for 12 h. After that, these tubes were slowly cooled down to 923 K. After annealing for 3 days at 923 K, these tubes were naturally cooled to room temperature. Finally, the ingots were pulverized into powders in agate mortars and sintered by spark plasma sintering (SPS, Sumitomo SPS-2040) at 723 K under a pressure of 65 MPa for 5 min. Electrically insulating and thermally conducting boron nitride layers were sprayed onto the surface of carbon foils before the SPS process in order to prohibit direct current (DC) pulsed currents going through powders.

The phase compositions in the prepared samples were identified by room-temperature powder X-ray diffraction measurements (RT-PXRD, Rigaku D/max 2550 V) with Cu Kα source. The sample morphologies and elemental distribution were measured by energy dispersive spectroscopy (EDS, Oxford Horiba 250). X-ray photoelectron spectroscopy (XPS, ESCALAB 250, Thermo Scientific) was used to identify the binding energies of each component elements. The σ and S of bar-shaped samples were measured simultaneously using a commercial system (ZEM-3, ULVAC). The κ was calculated according to the formula $\kappa = D \times C_p \times d$, where D is the thermal diffusivity, C_p is the heat capacity, and d is the density. Thermal diffusivity (D) was measured using the laser flash method (LFA-457, Netzsch) on a round specimen with the size of 10 mm in diameter and around 1.5 mm in thickness. The specific heat (C_p) was derived from the Dulong–Petit law, while the densities (d) were obtained by measuring the weights and volumes of the samples. The Hall coefficient (R_H) was measured by a physical properties measurement system (PPMS, quantum design). The hole p was calculated via $p = 1/eR_H$, where e is the elementary charge.

3 Results and discussion

The phase purity and crystal structure of the synthesized $Cu_{2-x}Li_xS$ ($x = 0$, 0.005, 0.010, 0.050, and 0.100) samples were examined by XRD with Cu Kα radiation at 300 K. As shown in Fig. 1, XRD patterns of $Cu_{2-x}Li_xS$ ($x \leq 0.05$) can be well indexed to the low-chalcocite phase (space group $P21/c$, PDF No. 83-1462). No other phases are detected. This suggests that doping Li at Cu-sites in Cu_2S does not change the structure symmetry of Cu_2S when $x \leq 0.050$. For $Cu_{1.9}Li_{0.1}S$ with a high Li-doping content, some new diffraction peaks are observed, which are indexed to $Cu_{1.96}S$ phase (space group $P4_32_12$, PDF No. 29-0578). In contrast with the good stability of those samples with Li-doping content $x \leq 0.05$, it is found that $Cu_{1.9}Li_{0.1}S$ is unstable in air. After polishing, the surface of the $Cu_{1.9}Li_{0.1}S$ bulk sample gradually changes from shiny to gray, which might be caused by the oxidation of Li elements. Thus, in the following part, only the electrical and thermal transport properties of those stable $Cu_{2-x}Li_xS$ ($x \leq 0.05$) samples are discussed.

For the Cu-deficient $Cu_{2-\delta}S$ compounds, the single low-chalcocite phase only exists in a very narrow composition range with $1.991 \leq \delta \leq 2.000$ at 300 K [7]. According to the Cu–S phase diagram, when δ is smaller than the limit value of 1.991, the Djurleite phase (space group $P4_32_12$, PDF No. 29-0578) appears and the $Cu_{2-\delta}S$ ($1.965 \leq \delta \leq 1.991$) becomes a mixture of the low-chalcocite phase and Djurleite phase [19]. Thus, the absence of Djurleite phase in our synthesized $Cu_{2-x}Li_xS$ ($x \leq 0.050$) samples proves that almost all Li dopants enter into the Cu-sites and the actual content of Cu-vacancy inside the crystal structure should be very small. However, due to the similar ionic radii between Li^+ (76 pm) and Cu^+ (77 pm) under the six-coordination [20], these Li dopants scarcely induce any peak shift in the XRD patterns of the Li-doped samples. Figure 2 presents EDS mappings of $Cu_{1.995}Li_{0.005}S$ and $Cu_{1.99}Li_{0.01}S$ samples. Owing to the light atomic mass, the signal of Li cannot be detected by EDS analysis. However, it is clear that Cu and S are homogeneously distributed inside the matrix without any elemental agglomeration or deficiency. This suggests that there are no Li-included secondary phases formed during the synthesis process. Combining the absence of Djurleite phase in XRD patterns (Fig. 1), it is reasonable to speculate that the real chemical compositions in the present $Cu_{2-x}Li_xS$ ($x \leq 0.05$) samples are close to the nominal chemical composition.

Figure 3 shows Cu 2p, S 2p, and Li 1s XPS spectra for $Cu_{1.95}Li_{0.05}S$. The Cu 2p XPS spectra consist of two peaks corresponding to the spin–orbit-split $2p_{3/2}$ and $2p_{1/2}$. For $Cu_{1.95}Li_{0.05}S$, the $2p_{3/2}$ and $2p_{1/2}$ peaks locate at 932.9 and 952.7 eV, respectively, which are almost the same with

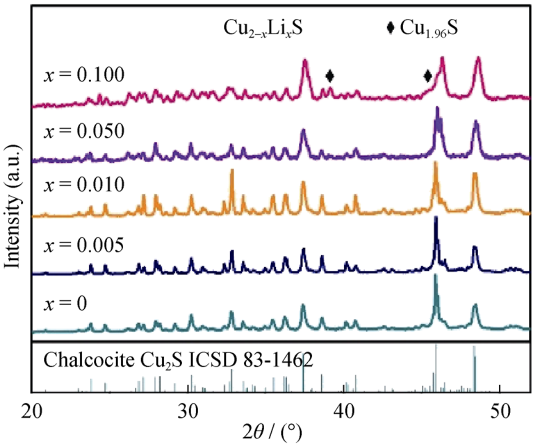

Fig. 1 Room-temperature powder XRD patterns for $Cu_{2-x}Li_xS$ ($x = 0$, 0.005, 0.010, 0.050, and 0.100) samples

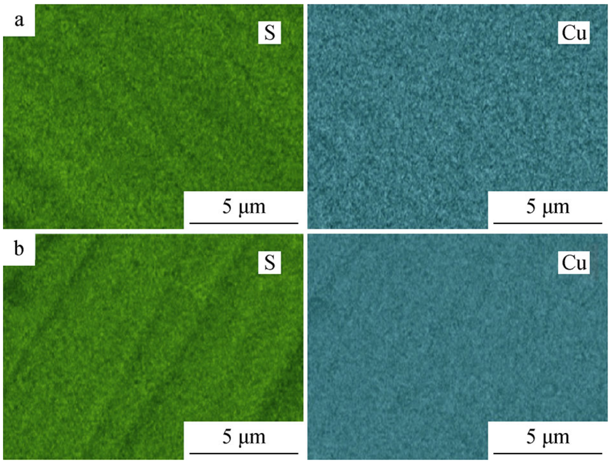

Fig. 2 Elemental EDS mappings of **a** $Cu_{1.995}Li_{0.005}S$ and **b** $Cu_{1.99}Li_{0.01}S$

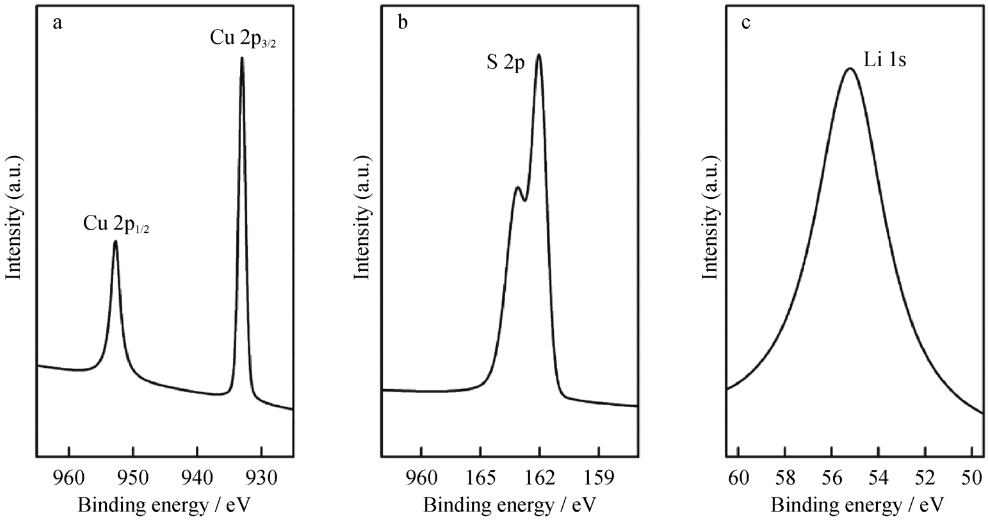

Fig. 3 XPS spectra for **a** Cu 2p, **b** S 2p, **c** Li 1s in $Cu_{1.95}Li_{0.05}S$

those of the pristine Cu_2S [13]. The S 2p binding energy in $Cu_{1.95}Li_{0.05}S$ is also the same with that in the pristine Cu_2S, suggesting that introducing Li in Cu_2S scarcely changes the valence states of Cu and S [13]. Likewise, the Li 1s signal is detected at 55.2 eV, slightly higher than those observed in the metallic Li [21]. Combining the above XRD and EDS analyses, it can be concluded that Li is doped in the samples prepared in this study.

Figure 4 shows the measured TE properties for the synthesized $Cu_{2-x}Li_xS$ ($x = 0$, 0.005, 0.010, and 0.050) samples, in which the overall measurement errors in the σ, S, and κ were estimated to be about ± 5%, ± 3%, and ± 7% [22]. All samples possess positive S throughout the entire measured temperature range, indicating that holes are the dominate carriers. The σ of Cu_2S is quite low with a value of about 0.1×10^4 $S{\cdot}m^{-1}$ at 300 K. This low σ is mainly contributed by the wide band gap (~ 1.2 eV) of Cu_2S [23]. As shown in Fig. 4a, b, with the increase in Li-doping content, S gradually decreases, while σ increases in the whole measured temperature range. For $Cu_{1.95}Li_{0.05}S$, the σ increases to about 0.87 $S{\cdot}m^{-1}$ at 300 K, about one order of magnitude higher than that of Cu_2S matrix. In contrast, the S value of $Cu_{1.95}Li_{0.05}S$ at 300 K is reduced to 80 $\mu V{\cdot}K^{-1}$, only a half as large as that of Cu_2S matrix. These lead to the significant enhancement of PF ($PF = S^2\sigma$) in the Li-doped samples, especially at temperatures above 600 K (Fig. 4c). The maximal PF value is about 6.4 $\mu W{\cdot}cm^{-1}{\cdot}K^{-2}$ at 800 K in $Cu_{1.95}Li_{0.05}S$, which is comparable with that observed in the Cu-deficient Cu_2S compounds [9]. Figure 4d shows that the κ values of all $Cu_{2-x}Li_xS$ ($x = 0$, 0.005, 0.010, and 0.050) samples have a weak temperature dependence. This is a common feature observed in almost all superionic TE materials reported so far, which might be related with the strong anharmonicity in these compounds [24–26]. The κ values of $Cu_{1.995}Li_{0.005}S$ and $Cu_{1.99}Li_{0.01}S$ are slightly higher than that of Cu_2S matrix. However, when the Li-doping content is raised to $x = 0.050$, κ is obviously increased. At 300 K, the κ value of $Cu_{1.95}Li_{0.05}S$ is about 0.84 $W{\cdot}m^{-1}{\cdot}K^{-1}$, around twice that of Cu_2S matrix.

The significantly improved electrical transport properties in $Cu_{2-x}Li_xS$ samples are very interesting. As mentioned above, XRD and EDS analyses confirm that almost all the Li dopants enter into the lattice of the $Cu_{2-x}Li_xS$ ($x \leq 0.05$) samples. Thus, the presence of secondary phases is ruled out as the reason for the improved electrical transport properties in the Li-doped samples. In Cu_2S, it is generally regarded that the valence states of Cu and S are + 1 and − 2, respectively [13]. Considering that Li only has one s electron in the outermost shell, it is expected that doping Li at Cu-sites should scarcely change the p. However, the Hall measurements shown in Fig. 5a suggest that the p increases with the increase in the Li-doping content. At 300 K, the p value of $Cu_{1.95}Li_{0.05}S$ is 1.5×10^{20} cm^{-3}, which is about one order of magnitude higher than that of the Cu_2S matrix. In Cu-based compounds, the p-type electrical transport behavior is mainly contributed by the presence of intrinsic Cu vacancies formed during the fabrication process [27, 28]. Doping Li at Cu-sites might change the Cu-vacancy formation energy and modify the content of Cu-vacancy inside the lattice, leading to the enhanced p in the Li-doped samples. However, the modification is very tiny, and thus, it cannot be detected by above XRD and EDS analyses. Similar phenomenon has also been observed in S-alloyed Cu_2Se system [29]. As a result of such significantly enhanced p, the σ of Li-doped Cu_2S is greatly increased although the carrier mobility (μ) is reduced somewhat (Fig. 5a). Lukashev et al. [30]

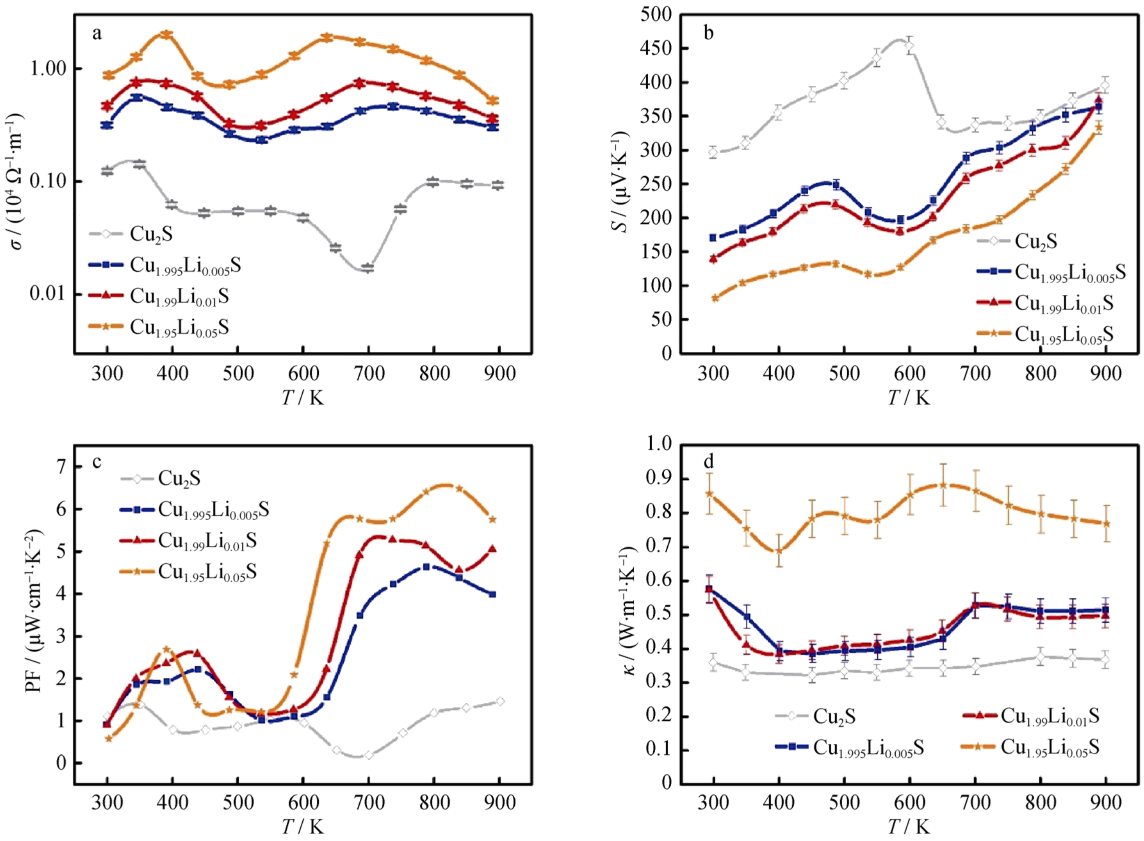

Fig. 4 Electrical and thermal transport properties of $Cu_{2-x}Li_xS$ ($x = 0.005$, 0.010, and 0.050) samples: **a** electrical conductivity (σ), **b** Seebeck coefficient (S), **c** power factor (PF), and **d** thermal conductivity (κ)

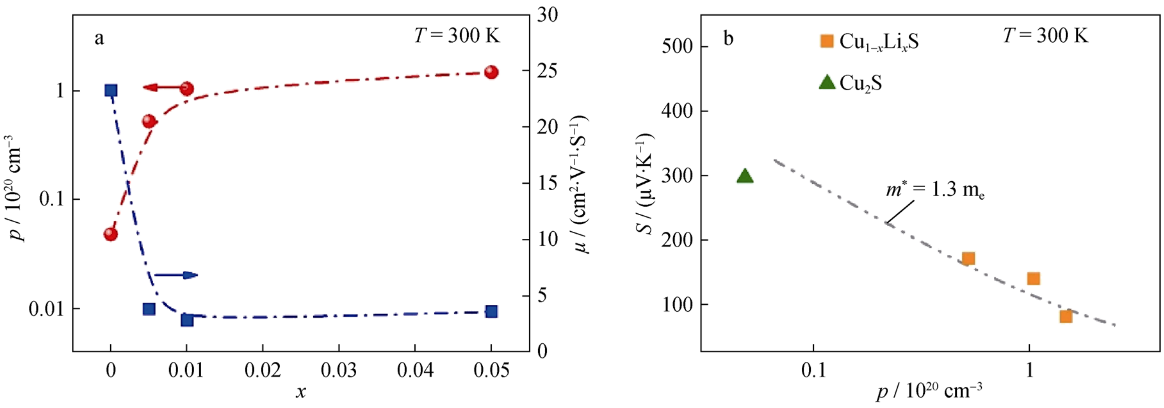

Fig. 5 **a** Hall carrier concentration (p) and Hall mobility (μ) as a function of Li-doping content for $Cu_{2-x}Li_xS$ ($x = 0$, 0.005, 0.010, and 0.050) samples; **b** experimental and calculated Pisarenko plots (S vs. p) at 300 K (line being calculated curve based on single-parabolic band model)

calculated the band structure of Cu_2S, and they found that the valence band maximum (VBM) is dominated by the Cu-d state and s state. Similar results have also been reported by Sun et al. [31] recently. However, due to the nature of the close shell d^{10} configurations of monovalent Cu, these d electrons have a very small contribution to the group velocity and the band shape in the valence band maximum [31]. Thus, the band shape of Cu_2S in VBM would be scarcely modified by the Li dopants. This can be confirmed by the Pisarenko plot (S *vs.* p) shown in Fig. 5b, which suggests that the Li-doped Cu_2S samples well follow the theoretical Pisarenko relation with the effective mass, $m^* = 1.3m_0$, where m_0 is the free electron mass. This result further proves the “electron crystal” feature of Cu_2S that the sulfur sublattice dominates the electrical transports, while the Cu atoms only provide electrons to determine the location of Fermi level.

Another abnormal phenomenon observed in Li-doped Cu_2S samples is the raised κ shown in Fig. 4d. The total κ of a solid is a sum of two contributions: the lattice thermal conductivity (κ_L) and the carrier thermal conductivity (κ_c). According to the Wiedemann–Franz law, the κ_c can be estimated by $\kappa_c = LT\sigma$, where L is the Lorenz number. Here, the L values are obtained by the following equation [32, 33],

$$L=\left(\frac{k_B}{e}\right)^2\times\left\{\frac{(\lambda+3)F_{\lambda+2}(\eta)}{(\lambda+1)F_\lambda(\eta)}-\left[\frac{(\lambda+2)F_{\lambda+1}(\eta)}{(\lambda+1)F_\lambda(\eta)}\right]^2\right\} \tag{1}$$

where k_B is the Boltzmann constant, e is the electron charge, λ is the scattering factor, and η is the reduced Fermi energy. The η can be calculated from the S by the equation,

$$S=-\frac{k_B}{e}\left[\eta-\frac{(\lambda+2)F_{\lambda+1}(\eta)}{(\lambda+1)F_\lambda(\eta)}\right] \tag{2}$$

where $\lambda = 0$ by assuming that the charge carriers are scattered by acoustic phonons in the present study. The Fermi integrals are given by $F_m(\eta)=\int_0^\infty \frac{x^m \mathrm{d}x}{1+\exp(x-\eta)}$, where x is the reduced carrier energy. The calculated L values are shown in Fig. 6a.

Based on these L values, the lattice thermal conductivities of the $Cu_{2-x}Li_xS$ samples from 300 to 900 K are shown in Fig. 6b. Clearly, the raised κ values presented in Fig. 4d are mainly contributed to the increased κ_L. This is quite abnormal because doping foreigner elements usually strengthens the point scattering to phonons and reduces the κ_L [34]. Although the atomic radii between Cu^+ and Li^+ under the six-coordination are similar [19], the different atomic masses should induce strong mass fluctuation and affect the normal transport of heat-carrying phonons. One possible reason for this abnormal phenomenon is the increased Cu ionic activation energy in Li-doped Cu_2S samples. In Cu_2S, the intrinsic ultralow κ_L mainly comes from the highly disordered migrating Cu ions inside the sulfur framework. Owing to the weak chemical bonding between Cu and S, these Cu ions possess very low ionic activation energies, about 0.19 eV in the hexagonal β-Cu_2S phase and 0.09 eV in the cubic α-phase, respectively [17]. Thus, these Cu ions can easily migrate among the sulfur sublattice with high diffusivities ($\sim 1\times10^{-5}$ $cm^2\cdot s$), which can strongly scatter the phonons and disrupt the normal heat propagation [17]. Doping Li significantly increases the ionic activation energy due to the “mixed mobile ions effect,” i.e., the ionic conductivity of a compound with more than one mobile ions will be drastically reduced compared to the single-ion conducting phase [17]. In 2004, Balapanov et al. [17] systematically investigated the effect of Li-doping on the Cu-ion migration behavior in Cu_2S. They found that the ionic conductivity of $Cu_{1.95}Li_{0.05}S$ is about one fourth that of Cu_2S matrix under the same temperature range. Correspondingly, the ionic activation energy of $Cu_{1.95}Li_{0.05}S$ is raised to 0.5 eV at 628 K, increasing by about 160% as compared with that of Cu_2S matrix. Thus, the Cu-ion short-range migration would be significantly suppressed in the present Li-doped samples, which will definitely lessen the phonon scattering and result in the high κ_L as shown in Fig. 5b.

Figure 7 shows the dimensionless zT calculated based on the measured σ, S, and κ, where the measurement errors in the zT were estimated to be about ± 12% [22]. Owing to the significantly optimized electrical transport properties, Li-doped Cu_2S samples demonstrate much improved zT as compared with the Cu_2S matrix despite the raised κ in these Li-doped samples. For $Cu_{1.99}Li_{0.01}S$, the maximum zT at 900 K is 0.84, about three times that of the Cu_2S matrix.

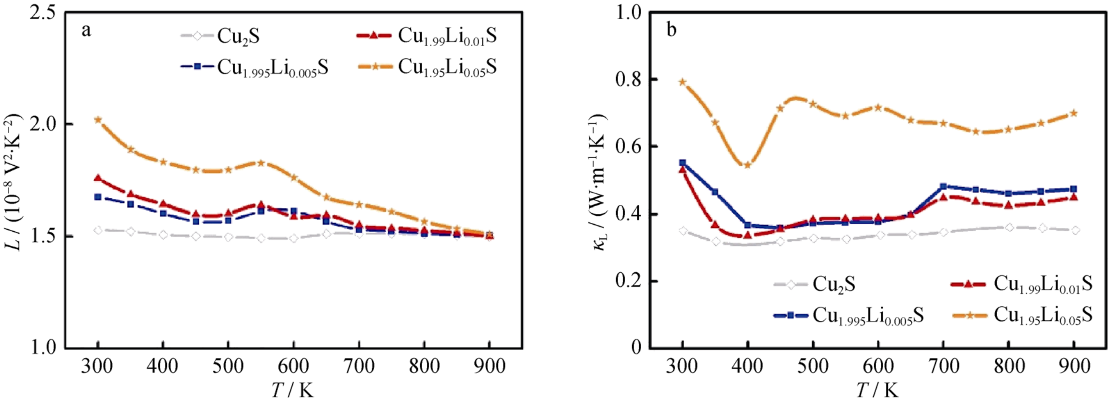

Fig. 6 Temperature dependences of **a** Lorenz number (L) and **b** lattice thermal conductivity (κ_L) for $Cu_{2-x}Li_xS$ (x = 0, 0.005, 0.010, and 0.050) samples

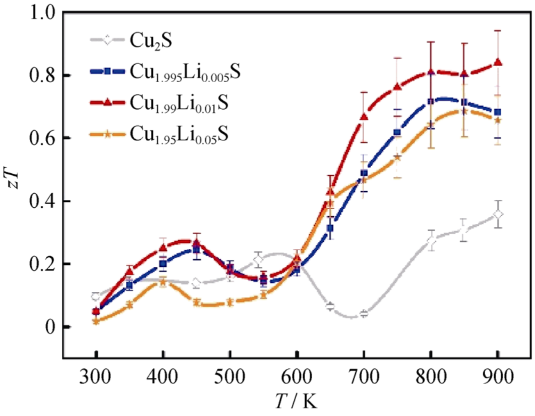

Fig. 7 Temperature dependence of TE figure of merit (zT) for $Cu_{2-x}Li_xS$ ($x = 0$, 0.005, 0.010, and 0.050) samples

4 Conclusion

In this work, a series of $Cu_{2-x}Li_xS$ samples with different Li-doping contents ($x = 0$, 0.005, 0.010, 0.050, and 0.100) were successfully synthesized. The effects of Li-doping on the phase composition, electrical, and thermal transport properties were investigated. It is found that the room-temperature crystal structure of Cu_2S can be well maintained until the Li-doping content reaches $x = 0.050$. Doping Li at Cu-sites significantly improves the p while scarcely modifies the initial band structure. Thus, the electrical transport properties in $Cu_{2-x}Li_xS$ have been significantly improved. For $Cu_{1.95}Li_{0.05}S$, the maximal PF is about 6.4 $\mu W \cdot cm^{-1} \cdot K^{-2}$ at 800 K, which is comparable with that observed in Cu-deficient Cu_2S compounds. Doping Li into Cu_2S suppresses the Cu-ion migration by increasing the ionic activation energy; thus, the κ values of $Cu_{2-x}Li_xS$ increase. As a result of the optimized electrical transport properties, a maximal zT of 0.84 at 900 K is obtained in $Cu_{1.99}Li_{0.01}S$, increasing by about 133% relative to that in the Cu_2S matrix.

Acknowledgements This work was financially supported by the National Natural Science Foundation of China (Nos. 51472262 and 51625205), the Key Research Program of Chinese Academy of Sciences (No. KFZD-SW-421) and the Shanghai Government (No. 15JC1400301).

References

[1] Snyder GJ, Toberer ES. Complex thermoelectric materials. Nat Mater. 2008;7(2):105.
[2] Li Z, Xiao C, Zhu H, Xie Y. Defect chemistry for thermoelectric materials. J Am Chem Soc. 2016;138(45):14810.
[3] Zeier WG, Zevalkink A, Gibbs ZM, Hautier G, Kanatzids MG, Snyder GJ. Thingking like a chemist: intuition in thermoelectric materials. Angew Chem Int Ed. 2016;55(24):6826.
[4] Shi X, Chen LD, Uher C. Recent advances in high-performance bulk thermoelectric materials. Int Mater Rev. 2016;61(6):379.
[5] Roy P, Srivastava SK. Nanostructured copper sulfides: synthesis, properties and applications. CrystEngComm. 2015;17(41):7801.
[6] Jiang QH, Yan HX, Khaliq J, Shen Y, Simpson K, Reece MJ. Enhancement of thermoelectric properties by atomic-scale percolation in digenite Cu_xS. J Mater Chem A. 2014;2(25):9486.
[7] Chakrabarti DJ, Laughlin DE. The Cu–S (copper–sulfur) system. Bull Alloy Phase Diagr. 1983;4(3):254.
[8] Will G, Hinze E, Abdelrahman ARM. Crystal structure analysis and refinement of digenite, $Cu_{1.8}S$, in the temperature range 10 to 500 °C under controlled sulfur partial pressure. Eur J Miner. 2002;14(3):591.
[9] He Y, Day T, Zhang TS, Liu HL, Shi X, Chen LD, Snyder GJ. High thermoelectric performance in non-toxic earth-abundant copper sulfide. Adv Mater. 2014;26(23):397.
[10] Zhao KP, Qiu PF, Song QF, Blichfeld AB, Eikeland E, Ren DD, Ge BH, Iversen BB, Shi X, Chen LD. Ultrahigh thermoelectric performance in $Cu_{2-y}Se_{0.5}S_{0.5}$ liquid-like materials. Mater Today Phys. 2017;1(1):14.
[11] Chen ZW, Jian ZZ, Li W, Chang YJ, Ge BH, Hanus R, Yang J, Chen Y, Huang MX, Snyder GJ, Pei YZ. Lattice dislocations enhancing thermoelectric PbTe in addition to band convergence. Adv Mater. 2017;29(23):1606768.
[12] He Y, Lu P, Shi X, Xu FF, Zhang TS, Snyder GJ, Uher C, Chen L. Ultrahigh thermoelectric performance in mosaic crystals. Adv Mater. 2015;27(24):3639.
[13] Qiu PF, Zhu YQ, Qin YT, Shi X, Chen LD. Electrical and thermal transports of binary copper sulfides Cu_xS with x from 1.8 to 1.96. APL Mater. 2016;4(10):104805.
[14] Qiu PF, Zhang TS, Qiu YT, Shi X, Chen LD. Sulfide bornite thermoelectric material: a natural mineral with ultralow thermal conductivity. Energy Environ Sci. 2014;7(12):4000.
[15] Li XY, Hu CG, Kang XL, Len Q, Xi Y, Zhang KY, Liu H. Introducing kalium into copper sulfide for the enhancement of thermoelectric properties. J Mater Chem A. 2013;1(44):13721.
[16] Zhang AJ, Shen XC, Zhang Z, Lu X, Yao W, Dai J, Xie DD, Guo LJ, Wang GY, Zhou XY. Large-scale colloidal synthesis of Cu_5FeS_4 compounds and their application in thermoelectrics. J Mater Chem C. 2017;5(2):301.
[17] Balapanov MK, Gafurov IG, Mukhamed'yanov UK, Yakshibaev RA, Ishembetov RK. Ionic conductivity and chemical diffusion in superionic $Li_xCu_{2-x}S$ ($0 \leq x \leq 0.25$). Phys Status Solidi B. 2004;241(1):114.
[18] Kang SD, Pöhls JH, Aydemir U, Qiu PF, Stoumpos CC, Hanus R, White MA, Shi X, Chen LD, Kanatzidis MG, Snyder GJ. Enhanced stability and thermoelectric figure-of-merit in copper selenide by lithium doping. Mater Today Phys. 2017;1(1):7.
[19] Potter RW. An electrochemical investigation of the system copper–sulfur. Econ Geol. 1977;72(8):1524.
[20] Shannon RD. Revised effective ionic radii and systematic studies of interatomic distances in halides and chalcogenides. Acta Crystallogr. 1976;A32(5):751.
[21] Kowalczyk SP, Ley L, McFeely FR, Pollak RA, Shirley DA. X-ray photoemission from sodium and lithium. Phys Rev B. 1973;8(8):3583.
[22] Duan B, Yang J, Salvador JR, He Y, Zhao B, Wang SY, Wei P, Ohuchi FS, Zhang WQ, Hermann RP, Gourdon O, Mao SX, Cheng YW, Wang CM, Liu J, Zhai PC, Tang XF, Zhang QJ, Yang JH. Electronegative guests in $CoSb_3$. Energy Environ Sci. 2016;9(6):2090.
[23] Marshall R, Mitra SS. Optical properties of cuprous sulfide. J Appl Phys. 1965;36(12):3882.
[24] Jiang BB, Qiu PF, Eikeland E, Chen HY, Song QF, Ren DD, Zhang TS, Yang J, Iversen BB, Shi X, Chen LD. Cu_8GeSe_6-based thermoelectric materials with an argyrodite structure. J Mater Chem C. 2017;5(4):943.

[25] Zhao KP, Duan HZ, Raghavendra N, Qiu PF, Zeng Y, Zhang WQ, Yang JH, Shi X, Chen LD. Solid-state explosive reaction for nanoporous bulk thermoelectric materials. Adv Mater. 2017;29(42):1701148.

[26] He Y, Zhang TS, Shi X, Wei SH, Chen LD. High thermoelectric performance in copper telluride. NPG Asia Mater. 2015;7(8):e210.

[27] Zhao LL, Wang XL, Fei FY, Wang JY, Cheng ZX, Dou SX, Wang J, Snyder GJ. High thermoelectric and mechanical performance in highly dense $Cu_{2-x}S$ bulks prepared by a melt-solidification technique. J Mater Chem A. 2015;3(18):9432.

[28] Ge ZH, Zhao LD, Wu D, Liu X, Zhang BP, Li JF, He JQ. Low-cost, abundant binary sulfides as promising thermoelectric materials. Mater Today. 2016;19(4):227.

[29] Zhao KP, Blichfeld AB, Chen HY, Song QF, Zhang TS, Zhu CX, Ren DD, Hanus R, Qiu PF, Iversen B, Xu FF, Snyder GJ, Shi X, Chen LD. Enhanced thermoelectric performance through tuning bonding energy in $Cu_2Se_{1-x}S_x$ liquid-like materials. Chem Mater. 2017;29:6367.

[30] Lukashev P, Lambrecht WRL, Kotani T, van Schilfgaarde M. Electronic and crystal structure of $Cu_{2-x}S$: full-potential electronic structure calculations. Phys Rev B. 2007;76(19):195202.

[31] Sun YX, Xi LL, Yang J, Wu LH, Shi X, Chen LD, Snyder GJ, Yang JH, Zhang WQ. The “electron crystal” behavior in copper chalcogenides Cu_2X ($X = Se$, S). J Mater Chem A. 2017;5(10):5098.

[32] May AF, Fleurial JP, Snyder GJ. Thermoelectric performance of lanthanum telluride produced via mechanical alloying. Phys Rev B. 2008;78(12):125205.

[33] Zhao KP, Blichfeld AB, Eikeland E, Qiu PF, Ren DD, Iversen BB, Shi X, Chen LD. Extremely low thermal conductivity and high thermoelectric performance in liquid-like $Cu_2Se_{1-x}S_x$ polymorphic materials. J Mater Chem A. 2017;5(34):18148.

[34] Chen YX, Ge ZH, Yin MJ, Feng D, Huang XQ, Zhao WY, He JQ. Understanding of the extremely low thermal conductivity in high-performance polycrystalline SnSe through potassium doping. Adv Funct Mater. 2016;26(37):6836.